Earth, Planets and Space

FULL PAPER Open Access

Pattern in ejecta curtain generated by the impact into granular targets of various sized particles and application to the ejecta curtain observed in the Hayabusa2 impact experiment

Toshihiko Kadono[1*], Ayako I. Suzuki[2], Ryo Suetsugu[3], Yuri Shimaki[4] and Sunao Hasegawa[4]

Abstract

We conducted impact experiments using targets composed of particles with size distributions and projectiles with a size larger than or comparable with the maximum size of particles in targets. The pattern and particle concentration in the ejecta curtain were investigated. The results show three types of ejecta curtain features: (i) filament pattern extending throughout the entire curtain and high concentration, (ii) filament pattern and low concentration, and (iii) mesh-like pattern with a structure on smaller scales than the entire curtain and low concentration. When the target consists of particles using a bimodal size distribution with size differences of more than one order of magnitude, the filament pattern appears, exhibiting case (i). If the target consists of particles with various sizes with size differences of more than one order of magnitude, the filament pattern appears, but the concentration decreases, appearing the features of case (ii). Case (iii) occurs when the target consists of particles with a single size or when the mass of particles with a certain size is dominant. Thus, the size distribution of the particles in the targets determines the pattern and particle concentration in the ejecta curtain. Based on these results, we confirm that the pattern in the ejecta curtain caused by the impact of the Small Carry-on Impactor (SCI) in the Hayabusa2 mission showing case (i) is consistent with the evaluated sizes and masses of grains and boulders in the ejecta curtain.

Keywords: Impact cratering, Ejecta curtain, Pattern formation, Size distribution, Asteroid Ryugu, SCI crater

*Correspondence: kadono@med.uoeh-u.ac.jp

[1] Department of Basic Sciences, University of Occupational and Environmental Health, Kitakyusyu, Japan
Full list of author information is available at the end of the article

Graphical Abstract

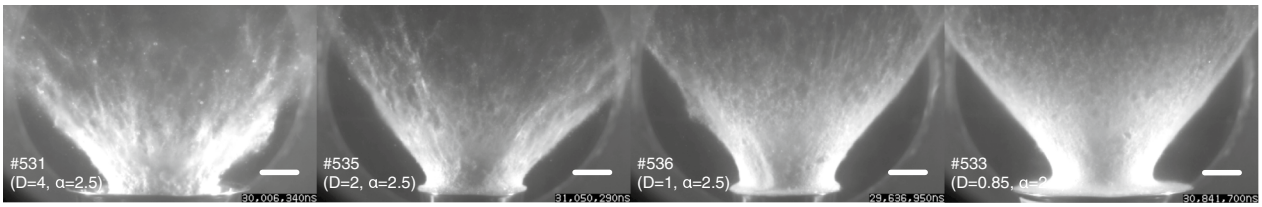

Introduction

The Japan Aerospace Exploration Agency (JAXA) Hayabusa2 spacecraft carried out remote sensing measurements of the C-type asteroid, Ryugu, and collected a large amount of data about the features of the Ryugu surface (e.g., Watanabe et al. 2019; Sugita et al. 2019; Kitazato et al. 2019; Okada et al. 2020). One of the important features revealed by onboard cameras was the presence of numerous large boulders, up to ~ 160 m on the surface of Ryugu (Sugita et al. 2019; Michikami et al. 2019). To excavate such a boulder-rich Ryugu surface, Hayabusa2 used an impactor, the Small Carry-on Impactor (SCI). The SCI impact experiment successfully created a crater (Arakawa et al. 2020). The diameter of the crater indicated that the crater formation occurred in the gravity regime (Arakawa et al. 2020), meaning that the surface of Ryugu can be regarded as a granular target without strength, even though it is composed of boulders of various sizes.

The in-situ observation of the ejecta curtain caused by the SCI impact showed that the pattern in the ejecta curtain had a complex filament structure [Fig. 1d in Kadono et al. (2020b). Kadono et al. (2015), Kadono et al. (2019), Kadono et al. (2020a)] have experimentally investigated the pattern in ejecta curtains in laboratories, using targets of single-size particles (glass beads, 50, 100, and 300 μm, and silica sand, 70 μm) and particles with bimodal size distributions (glass beads, 100 μm + 1 mm, 100 μm + 4 mm). The pattern in the ejecta curtains was significantly different: a mesh-like pattern appeared for targets of single-sized particles, whereas a complex filament pattern extending the entire curtain was observed for targets of particles with a bimodal size distribution. These results showed that the ejecta curtain caused by the SCI impact may not contain single-sized grains but large and small grains that vary in size by more than an order of magnitude, suggesting that the material in the ejecta curtain by the SCI impact was the sum of the material from the surface layer and the material from the subsurface layer of Ryugu (Kadono et al. 2020b).

In this study, two goals are set. The first is to experimentally investigate the dependence of the pattern in ejecta curtains on the size distribution of particles in the curtains. Then, based on this result, the second goal is to confirm that the material in the ejecta curtain caused by the SCI impact actually exhibits the corresponding conditions.

First, we conducted impact experiments to investigate the patterns in the ejecta curtain using targets with power-law size distributions at the same projectile and impact velocity as in the previous study. We examined the relationship between the size distribution of particles and the characteristic features in ejecta curtains. This was done by combining previous results for targets consisting of particles with a single size and bimodal distribution, as well as our results for targets of particles with a power-law distribution.

Crater formation processes such as cratering efficiency and ejecta distribution significantly change in the case that the size of target particles is larger than the size of the projectile (e.g., Cintala et al. 1999; Güttler et al. 2012; Tatsumi and Sugita 2018; Barnouin et al. 2019). This is

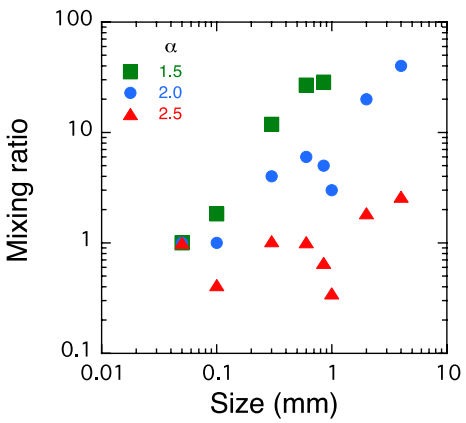

Fig. 1 Mixing ratio of glass beads. The total mass of glass beads for each size normalized by the total mass of 50 μm beads is shown as a function of bead sizes. The value of *α* is the power-law exponent of the cumulative number of target constituent glass beads. The ratio for each size is listed in Table 1

because target no longer behaves as a continuum and the shock wave is influenced by the individual particles, resulting in the rapid shock attenuation near the impact point (Barnouin et al. 2019). Since the diameter of the projectile used in our experiments was 4.8 mm and the upper limit of particle size in the targets was 4 mm, they are comparable. However, the gap between larger particles was filled by smaller particles and hence, target would behave like a continuum. Therefore, we expect that the patterns observed in this study were formed by processes in a continuous flow field.

Then, we applied the results to the ejecta curtain in the SCI impact experiment. Recently, the size distributions of the boulders at the surface and in the subsurface layer around the SCI impact crater were measured (Ogawa et al. 2022). Using this result, we verify whether the size distribution corresponding to the patterns in the ejecta curtain generated in the SCI impact are actually attained in the curtain.

Experiments

A polycarbonate sphere with a diameter of 4.8 mm (0.068 g in mass) was accelerated as a projectile by a vertical two-stage hydrogen-gas gun at the Institute of Space and Astronautical Science, JAXA. For targets, eight types of glass beads of different sizes were mixed such that the cumulative number of particles larger than the size of d was approximated as a power-law form $\sim d^{-\alpha}$, where α is a constant. Three distributions with different exponents α (1.5, 2.0, and 2.5) were prepared. The smaller the value of α, the greater the mass of larger sized particles, and the larger the value of α, the more evenly distributed the total mass of each particle is. The relative mass normalized by the total mass of 50 μm particles is shown in Table 1 and Fig. 1 as the mixing ratio for each exponent α. The maximum particle sizes D were set to 4, 2, 1, and 0.85 mm. The target conditions, α, and D, for each shot are listed in Table 2. For shots #531 to #533, the target was poured into a bowl with diameter and depth of 28 and 10 cm, respectively, having a flat bottom, and for shots #534 to #540, it was poured into a bowl with diameter and depth of 16.5 and 7 cm, respectively, also having a flat bottom. The vibration of the bowls was avoided as possible after mixing the particles to prevent segregation. The target was set in a vacuum chamber with an ambient pressure of less than 2.0 Pa during the impact. The nominal impact velocity was set to be 2.7 km/s. The ejecta motion was observed using a high-speed video camera (HPV-X, Shimadzu Co. Ltd) with a frame speed of 500 fps. The camera took neither any auto balancing of brightness nor adjusted gain. The size of a pixel taken by the camera was 1.1 mm/pix. The ejecta was illuminated using two halogen lamps perpendicular to the camera. A schematic experimental configuration is shown in Fig. 2.

Table 1 Mixing ratio of glass beads

Size mm	Mixing ratio		
	$\alpha = 1.5$	$\alpha = 2$	$\alpha = 2.5$
0.05	1	1	1
0.1	1.83	1	0.41
0.3	11.9	4	1.04
0.6	26.9	6	1.01
0.85	28.5	5	0.66
1		3	0.35
2		20	1.85
4		40	2.62

The ratio is represented as the total mass of glass beads for each size normalized by the total mass of 50 μm beads. The value of α is the power-law exponent of the cumulative number of target constituent glass beads

Table 2 Target conditions, α, and D, for each shot

Shot #	Max. size D (mm)	α
#531	4	2.5
#532	0.85	2.0
#533	0.85	2.5
#534	0.85	1.5
#535	2	2.5
#536	1	2.5
#538	4	2.0
#540	4	*

The target in the shot #540 consists of only 4 mm glass beads

*only 4 mm glass beads

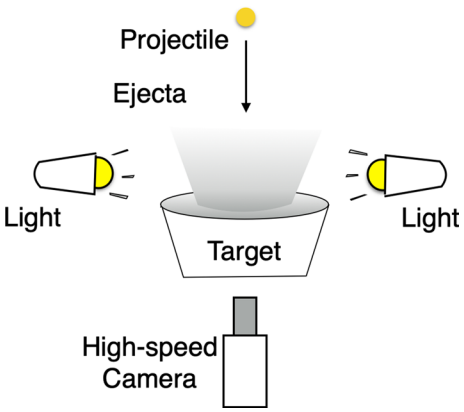

Fig. 2 Schematic diagram of the experimental setup. A polycarbonate projectile impacted perpendicularly to the target surface from the top in a vacuum chamber. Two-lights and high-speed camera were set outside the chamber

Results

A projectile from the top was impacted perpendicularly onto the surface of the granular target. Figure 3 shows snapshots of the ejecta at 28 ms after impact (video of each shot is shown in Additional files 2, 3, 4, 5, 6, 7, 8, 9, 10). It appears that there were clear differences in the patterns of the ejecta curtain. In the case of $D=4$ mm, when the slope α was small and the mass fraction of particles with the largest size was large (#538), the pattern was similar to the pattern for only 4 mm (#540). In contrast, when α was large (#531), where every size was assigned a similar mass, a filament pattern with high nonuniformity occurred. In the case of $D=0.85$ mm, when α was large and the mass fraction of the smaller particles was relatively large (#533), the pattern was similar to the characteristic pattern like a net for only 100 μm (e.g., Fig. 2

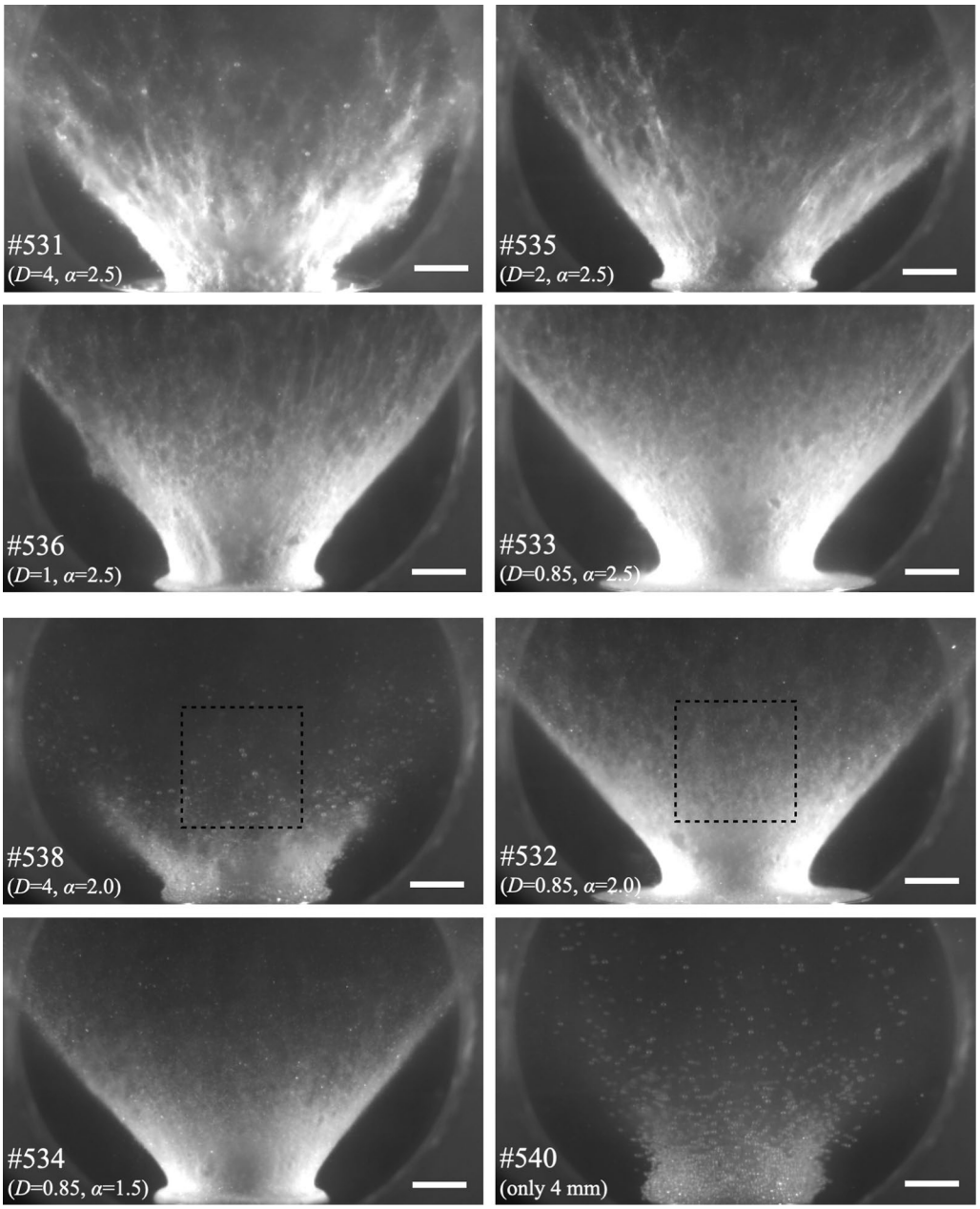

Fig. 3 Ejecta curtain captured by a high-speed camera at 28 ms after the impact. Projectile impacted vertically from the top. We investigated the intensity within an area in each image (examples of the area are indicated by the squares in the images of #532 and #538) to evaluate the spatial concentration of particles. The white horizontal line in each frame is a spatial scale indicating 50 mm

in Kadono et al. 2020a). When α was small and the mass fraction of 0.85 mm particles dominated, individual particles can be identified (the bright dots in the image of #534); the ejecta curtain became similar in the case for only 0.85 mm (e.g., Fig. 1, 2 12 in Tsujido et al. 2015). At a slope α of 2.5, the spatial structure of the ejecta curtain became nonuniform and filamentary as D increased (#531, #535, #536, and #533).

In shots #531–#533, the rim-to-time diameter of crater was ~ 20 cm (22.0, 20.0, and 21.0 cm, respectively), similar to the previous data (e.g., 20 cm for #422 in Additional file 1: Fig. S1 and 19 cm for #348 in Fig. S2). The fact that the crater size for targets consisting of particles with size distributions is similar for a target consisting of only 0.1 mm particles supports that the patterns observed in this study were formed by processes in a continuous flow field. On the other hand, in shots #534–#540, since the glass beads were placed in a bowl with a diameter of 16.5 cm, which was smaller than the final crater diameter under our impact conditions, the crater diameter could not be measured and the influence of the bowl sizes on crater formation process could not be evaluated from crater sizes. Nevertheless, we expect that the bowl size would not significantly affect the pattern in the ejecta curtain, because the growth rates of the neck of the ejecta curtain and the angle of ejecta curtain from target surface (~ 45°) that characterize the ejecta curtain were almost the same for shots #534–#540 and #531–#533 (Fig. 3).

Next, we considered the intensity contrast of the ejecta curtain in the images. The spatial concentration of the particles is reflected in the intensity distribution of the images. When the particles in the ejecta curtain are spatially concentrated, the intensity contrast should be high. To evaluate the intensity contrast, we analyzed the images using the same procedure by Kadono et al. (2019). We investigated the intensity I within the area of $N_0 = 100 \times 100$ pixels around the center of the ejecta curtain, and the area was fixed at the same position in the ejecta curtain in each image. Examples of the area are shown in the images of #532 and #538 in Fig. 3. Figure 4a illustrates the intensity distributions for #532 ($D = 0.85$ mm, $\alpha = 2.0$) (thin black curve) and #538 ($D = 4$ mm, $\alpha = 2.0$) (bold red curve) 28 ms after the impact. It appears that the distribution of #532 is broader, implying that the contrast is higher. Then, we examined the cumulative number of pixels with intensities smaller than I, N ($< I$). Figure 4b shows N ($< I$), using the same data as in Fig. 4a, which is normalized according to N_0 ($= 10^4$). The ratio of the intensities at N ($< I$)/N_0 of 0.9 and 0.1 (denoted I_{90}/I_{10}) is considered as an index of the intensity contrast. High values of I_{90}/I_{10} (corresponding to the broad distributions in Fig. 4a) indicate high intensity contrast and particle concentration, while low values (the narrow distributions) indicate a spatially uniform distribution of particles. Figure 4c shows I_{90}/I_{10} for each shot as a function of τ defined by t/t_0, where t is the time after the impact and t_0 is the characteristic crater formation time scale. The crater formation time t_0 can be defined as $(r/g)^{1/2}$, where g is the gravitational acceleration and r is the characteristic length of the crater. Various lengths can be defined as r, such as rim radius, rim diameter, and apparent diameter measured at an initial surface elevation, but in any case, r is of the order of ~ 10 cm for our impact conditions and t_0 is of the order of ~ 100 ms; therefore, we set t_0 to 100 ms [in Kadono et al. (2019), t_0 is also set to 100 ms]. For the targets with large α and D (#538) and only 4 mm beads (#540), the value of I_{90}/I_{10} is ~ 1.5 in both cases and the temporal behavior appears to be similar such that I_{90}/I_{10} slightly increases and then becomes constant. For the other shots, I_{90}/I_{10} at the early stages is ~ 2, and it gradually decreases. The value of I_{90}/I_{10} for the same D (#533, #532, and #534) increases as α decreases. Meanwhile, I_{90}/I_{10} for the same α (#531, #535, #536, and #533) appears to be almost same or slightly increases as D increases.

Discussion

Relationship between the pattern in ejecta curtain and the size distribution of particles

Kadono et al. (2019) show that for a target containing two types of particles, large inclusions (4 mm) and fine particles (0.1 mm), the pattern is filamentary (Fig. 1b in Kadono et al. (2019) and Additional file 1: Fig. S1 (#423); video of each shot in Additional file 7, 11, 12, 13: Fig. S1) and the intensity contrast I_{90}/I_{10} is quite high (> ~ 2.5) at the early stages (Fig. 2c in Kadono et al. 2019). On the other hand, for the target containing slightly smaller inclusions (1 mm) and fine particles (0.1 mm), the pattern is not filamentary [Fig. 1a in Kadono et al. (2019) and Additional file 1: Fig. S1 (#422)] and I_{90}/I_{10} is lower (< ~ 2) (Fig. 2c in Kadono et al. 2019). The latter case is similar to the results for the target containing only 1 mm particles [Additional file 1: Fig. S1 (#425) and Fig. 2c in Kadono et al. 2019] and only 0.1 mm particles (Additional file 1: Fig. S2 (#348) and Fig. 2c in Kadono et al. 2019). Moreover, in the case of the target that includes 4, 1, and 0.1 mm particles, the pattern is filamentary [Additional file 1: Fig. S1 (#429)] and I_{90}/I_{10} is lower (Fig. 2c in Kadono et al. 2019). Based on these results, we classify the features into three types: (i) the pattern in the ejecta curtain is filamentary and the intensity contrast is high (> ~ 2.5), (ii) the pattern is filamentary and the contrast is low (< ~ 2.5), and (iii) the pattern is not filamentary (but mesh-like) and the contrast is low. In our experiments, the results for only 4 mm particles (#540), small α and large D (#538), and large α and small D (#533 and #536),

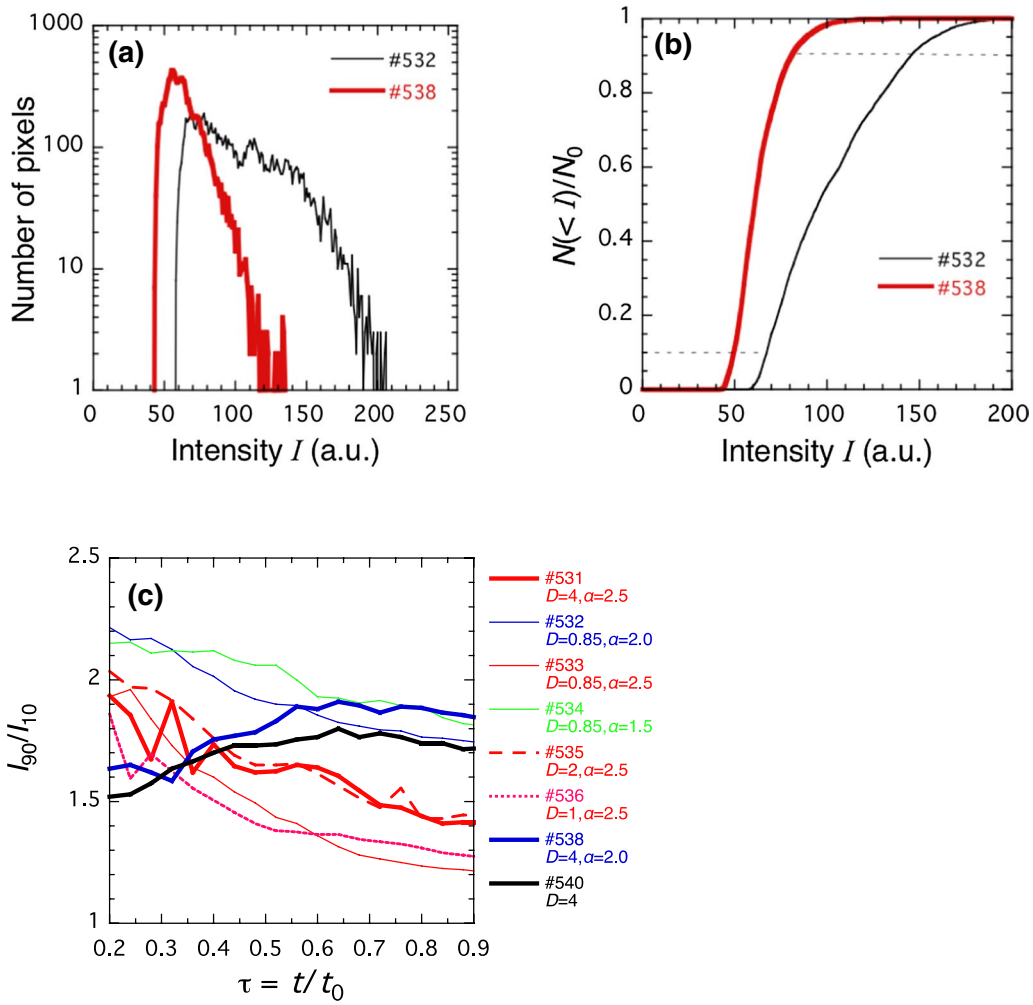

Fig. 4 **a** Intensity distributions at 28 ms after impact within the area with $N_0 = 100 \times 100$ pixels: #532 ($D = 0.85$ mm, $\alpha = 2.0$) (thin black curve) and #538 ($D = 4$ mm, $\alpha = 2.0$) (bold red curve). **b** Cumulative number of pixels with an intensity lower than I, $N(<I)$, normalized by N_0: #532 ($D = 0.85$, $\alpha = 2.0$) (thin black curve) and #538 ($D = 4$ mm, $\alpha = 2.0$) (bold red curve). The horizontal broken lines indicate $N(<I)/N_0$ of 0.9 and 0.1. **c** The ratio of the intensities at $N(<I)/N_0$ of 0.9 and 0.1, I_{90}/I_{10}. The horizontal axis is the normalized time τ, i.e., the time after the impact t divided by the characteristic crater formation time $t_0 = 100$ ms

correspond to case (iii), not filamentary (but mesh-like) and low contrast. Moreover, the results for small α and D (#532 and #534) also correspond to case (iii). On the other hand, the results for large α and D (#531 and #535) correspond to case (ii), filamentary and low contrast. Note that a mesh pattern like a net is observed in case (iii), and the spaces in the mesh pattern seem to increase as the maximum size of the particles contained by the target increases (e.g., #533 and #536 (Fig. 3); #348 (Additional file 1: Fig. S2) and #422 [Additional file 1: Fig. S1)]. The features of the pattern in the ejecta curtain and the particle conditions are summarized in Fig. 5.

Cases (i) and (ii) occur when the mass fractions of large and small particles are comparable, and the size range is over one order of magnitude. As the fraction of particles with intermediate sizes between these large and small sizes increases, the particle concentration decreases and the features of the ejecta curtain develop as in case (ii). On the other hand, even when the target consists of different-sized particles, if the size range is less than one order of magnitude and/or there is a characteristic size that dominates the mass fraction of particles, the pattern and particle concentration are similar to those for only particles of this size, i.e., case (iii). Thus, when the particles in the targets have different sizes, the pattern in the ejecta curtain depends on the dominant sizes of the particles in the targets.

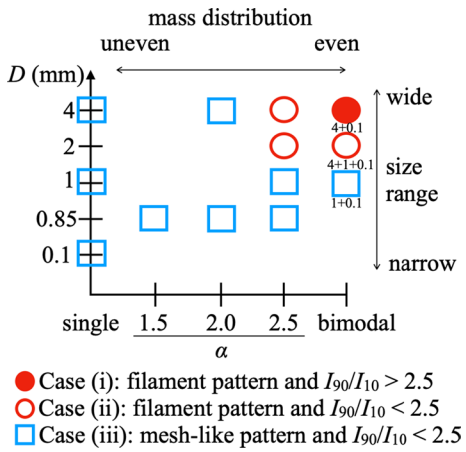

Fig. 5 Summary of the features of the pattern in ejecta curtains including the previous results (Kadono et al. 2019; Kadono et al. 2020a). The horizontal axis is the size distribution of particles and the vertical axis is the maximum size of particles. The closed circle, open circles, and open squares indicate case (i) (filament structure and $I_{90}/I_{10} > 2.5$), case (ii) (filament structure and $I_{90}/I_{10} < 2.5$), and case (iii) (mesh-like structure and $I_{90}/I_{10} < 2.5$), respectively. The result for the mixture of particles with 4, 1, and 0.1 mm is plotted as a bimodal distribution

The mutual inelastic collision of particles with fluctuating velocity during excavation has been proposed as a pattern formation mechanism (Kadono et al. 2015; Kadono et al. 2019; Kadono et al. 2020a; Nakazawa et al. 2021). In the case of targets with large inclusions, since their collision cross section is larger, the coalescence of small particles is promoted. If smaller particles effectively accumulate around larger particles, the particle concentration increases. When there are some particles with intermediate sizes between the largest and smallest sizes, since the small particles also accumulate around the intermediate sized particles, the concentration of small particles is reduced, and the particle concentration would decrease. If the mass fractions of large and small particles are comparable, the mutual influence on their motions becomes strong and the disturbance may develop into filamentary structures throughout the system.

Application to the ejecta curtain observed in the Hayabusa2 impact experiment

The size of the SCI projectile was 13 cm, whereas boulders of several meters were present near the SCI impact point on Ryugu surface (Arakawa et al. 2020; Ogawa et al. 2022). Fortunately, the projectile did not impact a large boulder directly, and a crater with a size that follows the conventional scaling law in the gravity regime was formed (Arakawa et al. 2020). This suggests that the SCI craters were formed in a continuous flow field. Therefore, in this section, we apply our experimental results obtained for targets with size distributions to the ejecta curtain formed by the SCI impact.

The pattern in the ejecta curtain caused by the SCI impact showed that the contrast I_{90}/I_{10} was quite high ($> \sim 3$) and then decreased (Fig. 2c in Kadono et al. 2020b). This exhibits the feature as in case (i), and hence, the ejecta curtain caused by the SCI impact may contain comparable mass fractions of large and small particles that vary in size by more than an order of magnitude. A detailed analysis of the observations shows that the ejecta curtain from the SCI impact consisted of grains of approximately a few centimeters (Wada et al. 2021) and boulders up to 1 m in size (Kadono et al. 2020b). The grains with a characteristic size of x_g approximately a few centimeters came from the subsurface layer of Ryugu and the boulders of $x_b \sim 1$ m came from the surface layer (Kadono et al. 2020b). The cumulative number distribution of grains larger than x per unit area in the subsurface layer, $N_g(>x)$, is represented by an exponential form (Ogawa et al. 2022), $\sim N_g(>x_g)e^{1-x/xg}$, and the total mass of grains per unit area in the subsurface layer M_g can be evaluated as $\sim x_g{}^3 N_g(>x_g)$. On the other hand, the cumulative number distribution of boulders larger than x per unit area on the surface of Ryugu, $N_b(>x)$, is represented by a power-law form (Sugita et al. 2019) as $\sim N_b(>x_b)(x/x_b)^{-\beta}$, where β is a constant. Hence, the total mass of boulders per unit area on the surface with a size smaller than x_b, M_b, is $\sim x_b{}^3 N_b(>x_b)$. Since the comparison between $N_g(>x)$ and $N_b(>x)$ shows that $N_g(>x_g)$ is $\sim 10^3$ times higher than $N_b(>x_b)$ (Ogawa et al. 2022), the total masses of grains of a few centimeters and 1 m boulders per unit area are comparable, $M_g \sim M_b$, because of $x_b \sim 10x_g$. This means that if the volume ejected by the SCI impact is the same in the surface and subsurface layers, the ejecta curtain would contain similar mass of grains of a few centimeters and boulders of ~ 1 m size. Conventional crater formation models show that target material shallower than approximately one-tenth of the crater diameter is excavated to be ejecta, while material deeper is displaced beneath the crater floor (e.g., Melosh 1989). In case of the SCI crater, the materials shallower than approximately 2 m or less are ejected [the rim diameter of the SCI crater is ~ 18 m evaluated by Arakawa et al. (2020)]. Since the thickness of the surface layer around the SCI crater is approximately 1 m (Arakawa et al. 2020), the volume ejected by the SCI impact is similar in the surface and subsurface layers. Therefore, the ejecta curtain may contain comparable mass fractions of materials from the surface and subsurface layers, i.e., grains of a few centimeters and boulders of ~ 1 m. Thus, we confirm that the size distribution of boulders and grains in the ejecta curtain caused by the SCI impact is consistent with the patterns exhibiting case (i). Note that,

this size distribution is a necessary condition for case 1, and it remains to be confirmed whether other conditions are satisfied for the actual grains in Ryugu to show such a pattern [e.g., restitution coefficient: It has been suggested that the restitution coefficient between particles is important for pattern formation (Kadono et al. 2015; Nakazawa et al. 2021)]. This is an issue for the future work.

Note also that in our experiment, particles of different sizes were mixed in the target before the impact, but in the SCI impact, the materials were separated in the surface and subsurface layers before the impact. However, conventional models of excavation flow suggest that, even when the target has the surface and subsurface layers, if each layer has no strength, the materials from the surface and subsurface layers are mixed in the ejecta curtain (e.g., Melosh 1989). Therefore, the experimental results can be applied to the SCI impact.

Summary

We conducted impact experiments using targets composed of particles with power-law size distributions and projectiles with a size larger than or comparable with the largest size of target particles, and investigated the pattern and particle concentration in the ejecta curtain. By combining our results with the previous results, we classified the features of the ejecta curtain into three types: (i) filament pattern and high concentration; (ii) filament pattern and low concentration; and (iii) mesh-like pattern and low concentration. If the target is a mixture of particles with size differences of more than one order of magnitude and the mass is evenly distributed over the size range, the pattern becomes filamentary, exhibiting case (i) or (ii). As the fraction of particles with intermediate sizes between the largest and smallest sizes increases, the concentration decreases and the feature of case (ii) appears. Case (iii) ensues when the target consists of particles with a single size or when the mass of the particles with a certain size is dominant. Thus, the principal sizes of the particles in the targets determine the pattern and particle concentration in the ejecta curtain. Based on the results of the laboratory experiments, we confirmed that the pattern in the ejecta curtain caused by the SCI impact in the Hayabusa2 mission exhibiting case (i) is consistent with the evaluated sizes of grains and boulders in the ejecta curtain, the size distributions of boulders around the SCI crater, the SCI crater size, and the layered structure around the SCI impact crater.

Note that the parameter range of the experimental results used in the discussion of this implication has been still narrow even including previous results. Therefore, future experiments should be conducted over a wider range of parameters to verify the conclusions of this study.

It is also noted that we consider the contrast of the image I_{90}/I_{10} as an index representing the pattern in ejecta curtain, but this method seems to have some limitations, e.g., #531 and #533, are obviously different in appearance (Fig. 3), but I_{90}/I_{10} is not so different in Fig. 4c. This may reveal that I_{90}/I_{10} alone is too simple to fully represent the difference. For more effective evaluation, quantitative pattern analysis using two-dimensional information would be effective. Moreover, different scattering properties of various sized particles should be included in the analysis. Although only qualitative interpretations are currently available, such quantitative analysis of the pattern would promote the studies of the pattern formation mechanism in the ejecta curtain. Furthermore, systematic numerical simulations would also further the quantitative studies of the mechanism in the future.

Supplementary Information

The online version contains supplementary material available at https://doi.org/10.1186/s40623-022-01672-9.

Additional file 1: Fig. S1. Ejecta curtain observed by Kadono et al. (2019) at 28 ms after the impact. Horizontal white bar indicates 50 mm. The impact conditions except for the target are the same as those in our experiment. **Fig. S2.** Ejecta curtain observed by Kadono et al. (2020a) at 28 ms after the impact. Horizontal white bar indicates 50 mm. The impact conditions except for the target are the same as those in our experiment.

Additional file 2: Video of shot #538

Additional file 3: Video of shot #532

Additional file 4: Video of shot #533

Additional file 5: Video of shot #535

Additional file 6: Video of shot #534

Additional file 7: Video of shot #425

Additional file 8: Video of shot #531

Additional file 9: Video of shot #536

Additional file 10: Video of shot #540

Additional file 11: Video of shot #429

Additional file 12: Video of shot #423

Additional file 13: Video of shot #422

Acknowledgements

The authors wish to thank M. Kiuchi for supporting the impact experiments. We are also grateful to two anonymous reviewers for their helpful comments. This work was supported by ISAS/JAXA as a collaborative program with the Hypervelocity Impact Facility.

Author contributions

All authors performed the impact experiments and contributed to data preparation, interpretation of results, and writing of the manuscript. TK designed the paper and completed the manuscript. All authors read and approved the final manuscript.

Funding

This study was not supported.

Availability of data and materials
The data sets used and/or analyzed during the current study are available from the corresponding author on reasonable request.

Declarations

Competing interests
The authors declare that they have no competing interests.

Author details
[1]Department of Basic Sciences, University of Occupational and Environmental Health, Kitakyusyu, Japan. [2]Department of Economics, Toyo University, Tokyo, Japan. [3]National Institute of Technology, Oshima College, Oshima, Japan. [4]Institute of Space and Astronautical Science, Japan Aerospace Exploration Agency, Sagamihara, Japan.

Received: 23 March 2022 Accepted: 28 June 2022
Published online: 19 August 2022

References

Arakawa M et al (2020) An artificial impact on the asteroid (162173) Ryugu formed a crater in the gravity-dominated regime. Science 368:67–71
Barnouin OS, Daly RT, Cintala MJ, Crawford DA (2019) Impacts into coarse-grained spheres at moderate impact velocities: implications for cratering on asteroids and planets. Icarus 325:67–83. https://doi.org/10.1016/j.icarus.2019.02.004
Cintala MJ, Berthoud L, Hörz F (1999) Ejection-velocity distributions from impacts into coarse-grained sand. Meteor Planet Sci 34:605–623
Güttler C, Hirata N, Nakamura AM (2012) Cratering experiments on the self-armoring of coarse-grained granular targets. Icarus 220:1040–1049. https://doi.org/10.1016/j.icarus.2012.06.041
Kadono T et al (2015) Crater-ray formation by impact-induced ejecta particles. Icarus 250:215–221. https://doi.org/10.1016/j.icarus.2014.11.030
Kadono T et al (2019) Pattern of impact-induced ejecta from granular targets with large inclusions. Astrophys J Lett 880:30. https://doi.org/10.3847/2041-8213/ab303f
Kadono T et al (2020a) Crater-ray formation through mutual collisions of hypervelocity-impact induced ejecta particles. Icarus 339:113590
Kadono T et al (2020b) Impact experiment on asteroid (162173) Ryugu: structure beneath the impact point revealed by in situ observations of the ejecta curtain. ApJ Letters 899:L22
Kitazato K et al (2019) The surface composition of asteroid 162173 Ryugu from Hayabusa2 near-infrared spectroscopy. Science 364:272–275
Melosh HJ (1989) Impact cratering: a geologic processes. Oxford University Press, New York
Michikami T et al (2019) Boulder size and shape distributions on asteroid Ryugu. Icarus 331:179–131
Nakazawa K, Okuzumi S, Kurosawa K, Hasegawa S (2021) Modeling early clustering of impact-induced ejecta particles based on laboratory and numerical experiments. Planet Sci J 2:237
Okada T et al (2020) Highly porous nature of a primitive asteroid revealed by thermal imaging. Nature 579:518–522
Sugita S et al (2019) The geomorphology, color, and thermal properties of Ryugu: implications for parent-body processes. Science 364:252
Tatsumi E, Sugita S (2018) Cratering efficiency on coarse-grain targets: implications for the dynamical evolution of asteroid 25143 Itokawa. Icarus 300:227–248
Tsujido S, Arakawa M, Suzuki AI, Yasui M (2015) Ejecta velocity distribution of impact craters formed on quartz sand: Effect of projectile density on crater scaling law. Icarus 262:79–92
Wada K et al (2021) Size of particles ejected from an artificial impact crater on asteroid 162173 Ryugu. Astron Astrophy 647:A43
Watanabe S et al (2019) Hayabusa2 arrives at the carbonaceous asteroid 162173 Ryugu—a spinning top-shaped rubble pile. Science 364:268–272
Ogawa K, et al. (2022) Boulder size distributions inside and around the artificial impact crater produced by Hayabusa2 SCI experiment on Ryugu. EPS submitted

Publisher's Note